Biochimica et Biophysica Acta 1837 (2014) 1625–1634

Contents lists available at ScienceDirect

Biochimica et Biophysica Acta

journal homepage: www.elsevier.com/locate/bbabio

Cationic screening of charged surface groups (carboxylates) affects electron transfer steps in photosystem-II water oxidation and quinone reduction

Oliver Karge [a], Ana-Nicoleta Bondar [b], Holger Dau [a,*]

[a] Inst. of Experimental Physics, Dept. of Physics, Free University of Berlin, Arnimallee 14, D-14195 Berlin, Germany
[b] Theoretical Molecular Biophysics, Inst. of Theoretical Physics, Dept. of Physics, Free University of Berlin, Arnimallee 14, D-14195 Berlin, Germany

ARTICLE INFO

Article history:
Received 24 March 2014
Received in revised form 14 July 2014
Accepted 16 July 2014
Available online 23 July 2014

Keywords:
Chlorophyll fluorescence
Electrostatic screening
Manganese complex
Oxygen evolution
Photosynthesis
Water oxidation

ABSTRACT

The functional or regulatory role of long-distance interactions between protein surface and interior represents an insufficiently understood aspect of protein function. Cationic screening of surface charges determines the morphology of thylakoid membrane stacks. We show that it also influences directly the light-driven reactions in the interior of photosystem II (PSII). After laser-flash excitation of PSII membrane particles from spinach, time courses of the delayed recombination fluorescence (10 μs–10 ms) and the variable chlorophyll-fluorescence yield (100 μs–1 s) were recorded in the presence of chloride salts. At low salt-concentrations, a stimulating effect was observed for the S-state transition efficiency, the time constant of O_2-formation at the Mn_4Ca-complex of PSII, and the halftime of re-oxidation of the primary quinone acceptor (Q_a) by the secondary quinone acceptor (Q_b). The cation valence determined the half-effect concentrations of the stimulating salt effect, which were around 6 μM, 200 μM and 10 mM for trivalent ($LaCl_3$), bivalent ($MgCl_2$, $CaCl_2$), and monovalent cations (NaCl, KCl), respectively. A depressing high-salt effect also depended strongly on the cation valence (onset concentrations around 2 mM, 50 mM, and 500 mM). These salt effects are proposed to originate from electrostatic screening of negatively charged carboxylate sidechains, which are found in the form of carboxylate clusters at the solvent-exposed protein surface. We conclude that the influence of electrostatic screening by solvent cations manifests a functionally relevant long-distance interaction between protein surface and electron-transfer reactions in the protein interior. A relation to regulation and adaptation in response to environmental changes is conceivable.

1. Introduction

In oxygenic photosynthesis, water provides the energized electrons (reducing equivalents) and the protons needed for carbon-dioxide reduction and carbohydrate formation [1,2]. The initial steps in the use of water as a raw material are facilitated by photosystem II (PSII), a multi-subunit protein-cofactor complex of impressive dimensions, which is embedded in the thylakoid membrane of plant, algae, and cyanobacteria. Sequential absorption of minimally four photons is required to oxidize two water molecules at the (electron) donor side of PSII ($2H_2O - 4e^- \rightarrow 4H^+ + O_2$) and to reduce two plastoquinone molecules at its acceptor side ($2Q + 4e^- \rightarrow 2QH_2$), rendering PSII a light-driven water–plastoquinone oxidoreductase. Water oxidation and plastoquinone reduction involve a total of six redox factors, all located at distinct sites within the PSII protein complex. Herein we investigate whether the variability of electrostatic surface potentials influences the protein-internal redox chemistry.

Today, results from biochemical and biophysical investigations [1,3–10] can be discussed in the light of the structural information that became available due to astounding progress in protein crystallography on PSII of thermophilic cyanobacteria [11–14]. The plant PSII resembles, most likely, the cyanobacterial PSII in all structural features that are functionally pivotal. A highly hydrophobic fraction of the PSII protein complex spans the thylakoid membrane and harbors all PSII pigments (chlorophylls, carotenoids and two pheophytins per PSII monomer), including the primary electron donor (P680) and primary acceptor (Phe). Yet a major fraction of the protein complex extends beyond the highly hydrophobic region. Whereas the extension of the membrane-spanning hydrophobic region of PSII measures around 30 Å only, the maximal extension of the PSII complex perpendicular to the membrane plane is around 100 Å (see, e.g., [9]). Aside from the ultra-fast primary photochemistry resulting in formation of the primary radical pair, [$P680^+$, Phe^-], all electron transfer steps and associated chemical reactions are taking place at redox factors located outside of the membrane-intrinsic protein region but still in the interior of the protein complex. The acceptor-side protein matrix harbors the primary and secondary quinone acceptors Q_a and Q_b. The redox-active tyrosine

* Corresponding author at: Tel.: +49 30 83853581.
E-mail address: holger.dau@fu-berlin.de (H. Dau).

http://dx.doi.org/10.1016/j.bbabio.2014.07.012
0005-2728/

Y_Z and the pentanuclear Mn_4Ca-oxo complex (Mn-complex) are located at the donor side of PSII. Absorption of a light quantum causes formation of the [$P680^+$, Phe^-] radical pair followed by electron transfer (ET) from Phe^- to Q_a within about 300 ps and from Y_Z to $P680^+$ within about 100 ns. Clearly later, in the microsecond and millisecond time domain, tertiary electron transfer steps are observable, which are in the focus of our investigation. At the acceptor side, the Q_b is reduced by Q_a^-. At the donor side, Y_Z^{ox} reduction is coupled to oxidation of the Mn-complex, which is thereby driven through its S-state cycle. For review of the processes outlined above, see, e.g., [5,6,8,10]. The transitions between four semi-stable S-states and their functionally crucial coupling to proton movements have been discussed in terms of an extended S-state cycle of alternating electron and proton removal from the Mn-complex [15–17].

The influence of thylakoid voltages and the resulting electric fields on the electron transfer steps in the interior of PSII has been investigated before [18–24]. The term 'thylakoid voltage' refers to the difference between the electric equilibrium potentials in the aqueous bulk phases separated by the thylakoid membrane, namely the stroma at the PSII acceptor and the lumen at its donor side. Whereas the role of delocalized membrane voltages has been considered before, mostly it has been assumed, at least implicitly, that the properties of the interface between protein and the surrounding aqueous solvent phase do not affect electron transfer between protein-internal redox factors significantly. However, by means of long-range electrostatic interactions, the charge distribution at the protein–solvent interface could affect both redox potentials and protonation states in the protein interior.

Numerous potentially charged amino-acid sidechains are found at the protein surface of PSII. A surprisingly high number of surface carboxylates (glutamate and aspartate sidechains) are present in the form of so-called carboxylate clusters [25,26]. In the present work, we will investigate whether electrostatic screening of the negatively charged surface groups by dissolved cations affects the electron transfer steps in the protein interior, at the acceptor and at the donor side of PSII.

In the research on plant photosynthesis, the role of surface charges and their screening by dissolved cations has been investigated intensively in the 1970s and 1980s. Seminal studies pursued in the seventies have resulted in the following picture. Screening of negative surface charges of photosynthetic membrane proteins, in particular located at PSII and associated light-harvesting complexes (LHCs), is a major determinant of the morphology of the thylakoid membrane system, specifically regarding the formation of membrane stacks (thylakoid stacking, e.g., [27,28]; for review, see [29,30]). In 1980, J. Barber summarized these findings and discussed the cationic screening comprehensively on grounds of the Gouy–Chapman theory of electric double-layer formation at charged surfaces [29]. Meanwhile dynamics changes of the thylakoid stacking have been related to a variety of adaptational and regulational phenomena, ranging from adaptation to light quality and intensity to the repair cycle of PSII, as reviewed in 2008 by Anderson, Chow, and De Las Rivas [30].

For a detailed discussion of the relation between surface charges, cation screening and surface potentials in the framework of the Gouy–Chapman theory, see [29,31]. Briefly, the presence of negatively charged surface groups is described by σ, the net surface charge density. Upon exposure of the charged surface to the electrolyte (that is, the ion-containing aqueous phase), a diffuse double layer of surface charges, solvent cations (majority), and solvent anions (minority) is formed. This double layer determines the effective electric potential at the surface (Ψ_0) as well as its decay length in the solvent phase. Increased cation concentration results in more efficient screening of the surface charges, meaning decreased (less negative) surface potential and decreased decay length in the solvent phase. Herein of special importance is the dependence on the ion valence. The ion concentration required for effective screening decreases strongly with increasing cation valence. Typically, 10–100 times lower concentrations are required for bivalent cations to achieve the same screening efficiency than for monovalent cations. The same holds true for trivalent cations compared to divalent cations. On the other hand, the screening efficiency is largely independent of the chemical type of the cation (similar effect of, e.g., Na^+ vs. K^+, Mg^{2+} vs. Ca^{2+}).

Following the lead of the investigations on the cation influence on thylakoid stacking, we use the cation-valence dependence and ion-type independence as a diagnostic tool to discriminate between influences originating from electrostatic screening, on the one hand, and binding to specific protein sites, on the other hand. The processes at the donor and acceptor side of PSII are tracked by time-resolved detection of the delayed fluorescence (recombination fluorescence) and the variable chlorophyll fluorescence yield of PSII after laser-flash excitation using the methodology described previously [32–34].

2. Materials and methods

2.1. Preparation of PSII samples

Samples of PSII-enriched membrane particles were prepared from spinach (*Spinacia oleracea*) as described elsewhere [35,36] and stored at −80 °C. Before and after freezing the samples exhibited an oxygen evolution activity of 1200–1400 μmol O_2 per mg chlorophyll (Chl) and hour at 28 °C, as determined polarographically on a Clark-type electrode under saturating white-light illumination using a combination of DCBQ (2,6-dichloro-*p*-benzoquinone) and ferricyanide as artificial electron acceptors [36,32].

Prior to fluorescence measurements, the PSII particles where thawed on ice for at least 1 h and washed twice by dilution in low-salt measuring buffer (1 M betaine, 5 mM MES, pH 6.2) and subsequent centrifugation. The pH was adjusted to 6.2 by addition of about 2.2 mM NaOH. Consequently, in all experiments reported herein, 2–3 mM of sodium ions were present already before supplementing the suspension by addition of salts at the indicated concentrations. The final pellet was suspended in low-salt measuring buffer and the sample concentration was adjusted to 1 mg Chl/ml. This stock suspension of PSII in low-salt buffer was stored on ice and kept in the dark until measurement.

To measure the effect of different cations on the time courses of prompt and delayed chlorophyll fluorescence, salt buffer suspension were prepared containing 1 M betaine, 5 mM MES (pH 6.2) and one of the following chlorides: NaCl, KCl, $MgCl_2$, $CaCl_2$, $LaCl_3$. On minute before start of the measurement, the respective salt buffer was mixed thoroughly with an aliquot of the PSII suspension and an artificial electron acceptor resulting in a concentration of 10 μg Chl/ml in the measuring suspension and a DCBQ concentration of 20 μM.

2.2. Prompt and delayed Chl fluorescence

Time-resolved measurements of the delayed fluorescence (delayed chlorophyll fluorescence) were done using the set-up described elsewhere [32,33]. Time-courses of the variable yield of the prompt chlorophyll fluorescence were measured employing a commercial instrument (Dual-Modulation Kinetic Fluorometer, FL-3000, Photon System Instruments Brno, Czech Republic), which was adopted for application of saturating ns-laser flashes to the PSII sample suspension [32,33,37].

To measure the delayed fluorescence, a sequence of 32 saturating laser flashes of nanosecond duration (532 nm, half-width of about 5 ns, 2 mJ/cm^2, period between flashes of 700 ms) was applied to the dark adapted PSII membrane particles and time courses of the delayed-fluorescence intensity were recorded, applying logarithmic averaging along the time axis immediately after data acquisition [32,33,37]. Scattered laser light was blocked by a combination of two long-pass filters with cut-off wavelength of 600 nm and 632 nm. All measurements were done at room temperature.

The data were corrected by subtraction of an artifact that resulted from excitation and subsequent delayed fluorescence emission of the glass and/or cathode material of the photomultiplier caused by the

strong prompt fluorescence of the PSII particles as well as by scattered light of the excitation flash. Details and procedure of this correction are described elsewhere [32,33,37].

The intensity of the delayed fluorescence, $F_R(t)$, depends on the concentration (fraction) of PSII with reduced quinone acceptor ($[Q_a^-]$) and oxidized chlorophyll donor ($[P680^+]$) as well as on the difference in Gibbs free energy, ΔG^{P+Q-}, between the excited antenna state and the $[P680^+\ Q_a^-]$ radical-pair state. To a good approximation, $F_D(t)$ can be described as follows:

$$F_D(t) = c_{exp} \cdot \exp\left(\Delta G^{P+Q-}/k_B T\right) \cdot \left[P680^+\right](t) \cdot [Q_a^-](t), \quad (1)$$

where c_{exp} is a time-independent experimental constant and k_B is the Boltzmann constant. After excitation by a light flash and rapid formation of $P680^+$ and Q_a^-, their concentration is monotonously decreasing due to subsequent electron and proton transfer steps. We note that also a time dependence of the value of ΔG^{P+Q-} is not excluded. Eq. (1) is based on the transient presence of a thermal-equilibrium distribution of the populations of radical-pair state and excited antenna state. Moreover, mutual independence of the $P680^+$ reduction and Q_a^- oxidation kinetics as well as a linear relation between the Q_A^- redox state and the prompt fluorescence yield is assumed. Taking into account that the changes in $F_D(t)$ extent over four orders of magnitude, Eq. (1) likely represent a good approximation [32].

The decrease in delayed-fluorescence intensity in the time domain of interest is predominantly determined by $[P680^+](t)$ and, to a lesser extent, by $[Q_a^-](t)$ [33]. To simplify the analysis, we correct for contribution of $[Q_a^-](t)$ to the time courses of $F_D(t)$. Due to the close relation between $[Q_a^-]$ and the prompt fluorescence yield, the time courses of delayed fluorescence can be corrected according to Eq. (2):

$$F_D^{corr}(t) = F_D(t)\left(\frac{F_M - F_0}{F_P(t) - F_0}\right), \quad (2)$$

where F_M is the maximum and F_0 is the minimum level of prompt fluorescence [38,33]. The value of F_M corresponds to $F_P(0)$ as obtained by extrapolation of a three-exponential fit of $F_P(t)$; F_0 was detected immediately before application of the 1st flash of the respective flash sequence.

This Q_a^- correction eliminates, to a first approximation, the contribution to the delayed-fluorescence decay stemming from the $[Q_a^-]$ decay [33]. We note that this correction does not necessarily eliminate all acceptor side contributions to the decay because also ΔG^{P+Q-} might be time-dependent due to processes at the acceptor side of PSII.

2.3. Data analysis

The time courses of prompt fluorescence as well as the Q_a^--corrected time courses of the delayed fluorescence were simulated using a sum of three exponential functions:

$$F(t) = \left(\sum_{i=1}^{3} A_i \exp(-t/\tau_i)\right) + c \quad (3)$$

The parameters A_i, τ_i, and c were determined by a least-square fit. The simulation results determined for prompt fluorescence decays were used (inter alia) to correct the delayed-fluorescence data for the influence of the $[Q_a^-]$ decay. The difference in Gibbs free energy of the $S_3^+ \rightarrow S_3^n$ transition was calculated from the parameters obtained by curve-fitting of the 3rd-flash transient of the Q_a^--corrected delayed fluorescence according to:

$$\Delta G = -k_B T \ln \frac{\sum_{i=1}^{3} A_i + c}{A_3 + c}. \quad (4)$$

3. Results

3.1. S-state transition probability

Dark-adapted PSII particles were excited by a sequence of saturating laser flashes (5 ns, 532 nm). After each flash, the delayed fluorescence (DF) was recorded within a time window of 10 μs to 10 ms. The DF intensity recorded at 2 ms after each flash exhibits a period-of-four pattern (Fig. 1) which resembles closely the flash pattern of dioxygen formation recorded by an oxygen electrode [39,40]. The period-of-four pattern of O_2-formation has been explained in 1970 by Kok and coworkers in terms of the meanwhile classical S-state model [40], as reviewed elsewhere [41]. Briefly, dark-adapted samples of PSII particles reside mainly in the fully dark-stable S_1 state. Depending on the extension of the dark-adaptation period, a minor fraction of photosystems may be in the S_0 state. In the herein reported experiments, extensive dark adaptation had resulted in a negligible initial S_0-state population. The first laser flash initiates advancement towards the S_2 state; the second flash induces the $S_2 \rightarrow S_3$ transition. The third flash initiates the transition from the S_3 state via a hypothetical S_4 state towards the S_0 state; the latter transition is coupled to dioxygen formation and release. The fourth flash induces the $S_0 \rightarrow S_1$ transition. Thereby the initial state present in dark-adapted PSII, the S_1 state, is reached again. Subsequent flashes drive the PSII repeatedly through Kok's reaction cycle so that, for perfectly synchronized advancement in the S-state cycle, dioxygen formation is observed on the 3rd, 7th, 11th, and 15th flash. However, as clearly visible in Fig. 1, the maxima at the 7th, 11th, and 15th flash are of lower amplitude and shifted towards the 12th, and 16th flash. This phase shift and damping of the oscillation reflects desynchronized S-state transitions due to 'misses'. The miss events are described quantitatively by the miss factor, which provides the mean probability for a failure of the PSII to advance in the S-state cycle. The miss factor (m) relates directly to the yield (Φ_t) of the processes occurring after initial formation of the $[P680^+, Q_a^-]$ radical pair:

$$\Phi_t = 100\% - m. \quad (5)$$

Visual inspection of the flash patterns shown in Fig. 1 reveals that the miss probability is affected by the salt concentration. Without addition

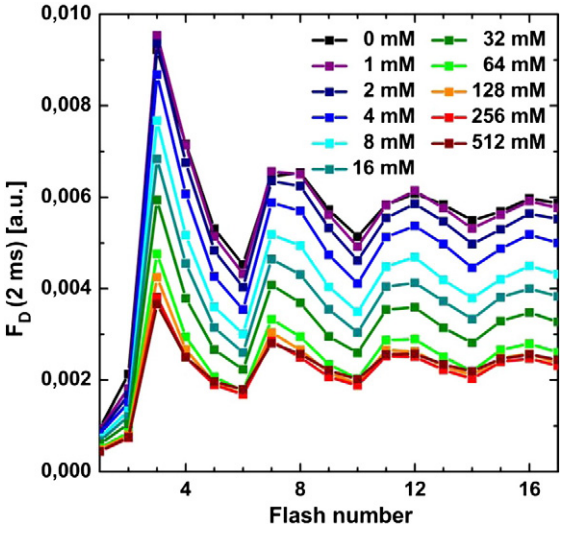

Fig. 1. Flash-number dependence of the delayed fluorescence (DF) intensity at 2 ms for a train of saturating laser flashes applied to dark-adapted PSII membrane particles. The DF intensity was averaged from 1 to 3 ms after application of the saturating laser flash (~5 ns FWHM, 532 nm, 2 mJ/cm^2). Data points are shown for 11 concentrations of NaCl; for better visualization, the data points were connected by solid lines. (There is a clear salt-dependence of the oscillation amplitudes, which is addressed further below.)

of NaCl (0 mM), the maximum at the 7th flash is shifted to the 8th flash indicating an especially high miss factor at very low salt concentrations. The third maximum is found on the 11th flash only in the pattern measured at a NaCl concentration of 128 mM. Otherwise the 3rd maximum is at the 12th flash, indicating that at 128 mM the lowest miss factor is reached. For quantitative analysis, the flash patterns were simulated using Kok's approach with 100% S_1 state population before flash application, and nil double-hit probability due to use of ns-laser flashes. (The S_0 state population is negligibly small due to extensive dark-adaptation during (i) preparation of the PSII-membrane particles and (ii) the washing steps in salt-free buffer solutions. Inclusion of an S_0-state population in the flash-pattern simulation resulted in insignificant S_0-levels only.)

Essentially the same flash patterns were obtained for KCl. For bivalent ($MgCl_2$, $CaCl_2$) and trivalent ($LaCl_3$) cations qualitatively the same effects were observable, but in different concentration ranges. The resulting miss factors are shown, for the five salts, in Fig. 2.

For all investigated salts, the concentration dependence of the miss factor is found to be biphasic. For rising salt concentrations, the miss factor first decreases from 13–15% at the low-salt level to 7–8% at intermediate-salt level followed by an increase towards the highest investigated salt concentrations. This behavior is observed for all five salts, but the respective concentration ranges depend on the cation valence. The half-value concentration of the miss-factor decrease is around 7 μM for the trivalent cation (La^{3+}), but is roughly 30 times higher for the bivalent cations (around 200 μM for Mg^{2+} and Ca^{2+}) and more than 1000 times higher for the monovalent cations (around 10 mM for Na^+ and K^+). Similarly also the concentrations of maximal transition efficiency depend pronouncedly on the valence of the cation. Maximal efficiencies were found around 300 μM, 7 mM and 150 mM. The herein observed dependency on the cation valence suggests that the investigated salt effect results from electrostatic screening of negatively charged groups at the protein surface (see also Section 4 Discussion).

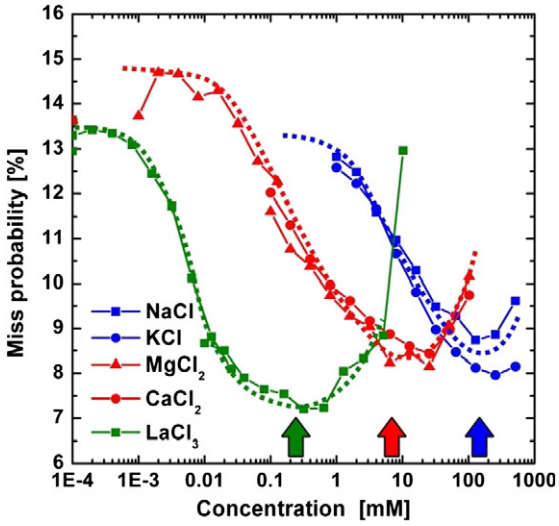

Fig. 2. Dependence of the miss probability, *m*, on salt concentration. The value of *m* was determined by simulation of the flash pattern of the delayed-fluorescence intensity at 2 ms after the saturating laser flash (see Fig. 1). The dotted lines do not represent any specific mathematical function, but were drawn to guide the eye. The following color coding was used: Blue: monovalent cations (Na^+, K^+); red: bivalent cations (Mg^{2+}, Ca^{2+}); green; trivalent cation (La^{3+}). The approximate concentration at the minimum of the miss factor is indicated by colored marker arrows. We note that seven concentration series are presented which were collected on seven different days; the points of each single series are connected by a solid line. In these seven concentrations series, the maximal values of the miss parameter at very low salt concentrations and its minimal values at intermediate concentrations are similar, but not identical. This is explainable by minor variations in the properties of the used PSII preparations.

3.2. Delayed fluorescence decays — qualitative discussion

3.2.1. '$S_3 \rightarrow S_0 + O_2$' transition induced by the 3rd flash

The DF intensity detected at 2 ms after each laser flash (Fig. 1) was used to determine the salt-dependence of the miss factor (Fig. 2). Complete time courses of the delayed fluorescence detected after the 3rd flash are shown in Fig. 3A. These DF transients have been corrected for the decay in the concentration of reduced Q_a^- (see Section 2 Materials and methods). Based on previous investigations [32,42,33,43,44], we can interpret these 3rd flash transients in terms of events at the donor side of PSII, using the S-state nomenclature introduced in [45]. Four points are noteworthy:

(1) At 10 μs after the laser flash, the primary quinone acceptor (Q_a) is reduced (Q_a^-) and the redox-active tyrosine at the donor side of PSII (Y_Z) is oxidized (for simplicity, the formally neutral tyrosine radical state is denoted as Y_Z^+). The DF intensity at 10 μs thus reflects the free energy level of the [Y_Z^+ Q_a^- S_3^+] state (that is,

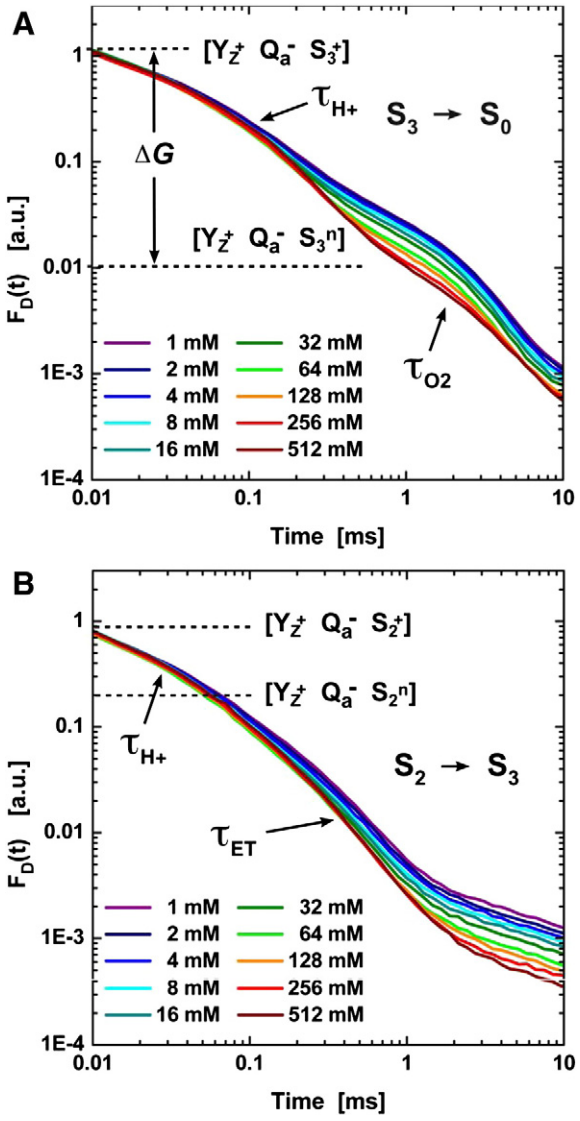

Fig. 3. Time courses of delayed PSII fluorescence recorded after application of a saturating laser flash (2 mJ/cm², 5 ns FWHM, 532 nm) at various NaCl concentrations. (A) The shown time courses were recorded after the 3rd laser flash inducing the $S_3 \rightarrow S_0$ transition and (B) after the 2nd flash inducing the $S_2 \rightarrow S_3$ transition (in B). The time courses for 11 concentrations of NaCl are shown. The data were corrected for the influence of Q_a^- reoxidation. The DF intensities at 10 μs are essentially unaffected by the salt concentration; the time courses were not normalized.

the [Q_a^- Y_Z^+] radical pair in the presence of the S_3^+ state of the Mn complex). Visual inspection of Fig. 3A shows that this energy level is unaffected by changes in the salt concentration.

(2) The 3rd-flash DF decay in the time domain from 10 μs to about 300 μs has been assigned to proton removal from the Mn-complex, in the $S_3^+ \rightarrow S_3^n$ transition [46,42,43]; no salt effect on its rate is visible. Thus, Fig. 3A suggests that the rate of proton removal from the Mn complex is not significantly affected by changes in the salt concentration.

(3) The DF level reached at about 1 ms reflects the Gibbs free energy after proton removal, that is, the energy of the state [Y_Z^+ Q_a^- S_3^n]. This level is decreasing significantly with increasing salt concentration (Fig. 3A); and consequently the Δ*G* of the proton removal step is increasing.

(4) The subsequent DF decay in the time domain from 1 to 10 ms, which reflects the time constant of dioxygen formation and $S_3 \rightarrow S_0$ transition, also appears to be affected by the salt concentration. However, mere visual inspection is insufficient to unravel the salt-dependence of τ_{O2}. Therefore, simulation (curve-fitting) of these transients has been approached, as discussed further below.

3.2.2. '$S_2 \rightarrow S_3$' transition induced by the 2nd flash

Fig. 3B shows the salt-effect on the DF transients of the $S_2 \rightarrow S_3$ transition induced by the second laser flash applied to dark-adapted PSII particles. We will approach a qualitative analysis of four aspects of the 2nd-flash DF transients based, inter alia, on very recent findings on proton removal in the $S_2 \rightarrow S_3$ transition [17].

(1) Upon laser-flash application in the S_2 state, the initial DF level, at 10 μs, and thus the Gibbs free energy level of the [Q_a^- Y_Z^+] radical pair appear to be fully unaffected by the increase in salt concentration (as is the case in the S_3-state).

(2) After formation of the initial [Y_Z^+ Q_a^- S_2^+] state, deprotonation and proton removal from the Mn-complex take place with a time constant (τ_{H+}) of about 30 μs resulting in formation of the [Y_Z^+ Q_a^- S_2^n] state. Fig. 3B shows that the rate constant ($k_{H+} = \tau_{H+}^{-1}$) of this proton-removal step is essentially unaffected by changes of the salt concentration.

(3) Subsequently, the electron transfer from the Mn-complex to the oxidized Y_Z^+ takes place resulting in formation of the [Y_Z^0 Q_a^- S_3^+] state. Its DF level around 2 ms and thus its free-energy level appear to decrease continuously with increasing salt concentrations. Between 2 ms and 10 ms the DF level decreases further, although no processes at the donor side have been reported to take place in this time domain. This decrease may either stem from imprecise or systematically inaccurate correction for the Q_a^- decay or result from a change of the ΔG_{P+Q-} due to processes at the acceptor side.

(4) At room temperature in a standard buffer, the time constant of the $S_2^+ \rightarrow S_2^n$ transition is around 300 μs. Visual inspection of Fig. 3B suggests that this ET step is slower at low salt concentrations and accelerated by increasing the salt concentration.

We do not attempt a similar discussion of the 1st-flash and 4th-flash DF time courses. The DF transients of the $S_1 \rightarrow S_2$ (1st flash) and $S_0 \rightarrow S_1$ (4th flash) are of significantly lower amplitude than the 2nd-flash and 3rd-flash transients, presumably explainable by lower free-energy levels in the presence of the uncharged Mn-complex in its S_1^n and S_0^n states (versus the charged S_2^+ and S_3^+). Therefore, the influence of S-state mixing (specifically in the 4th-flash transient) and a presently inevitable laser-flash artifact renders analysis of these time courses too problematic.

3.3. Rate constant of dioxygen formation

The DF time courses were simulated by a sum of three exponential functions (Eq. (3)) and the parameters A_i, *c*, and τ_i were determined by error-sum minimization. The slowest time constant provides the inverse rate constant of the dioxygen formation step ($\tau_3 = \tau_{O2} = k_{O2}^{-1}$); its salt concentration dependence is shown in Fig. 4. The corresponding amplitude (A_3) of this millisecond component of the DF decay ($A_3 = A_{ms}$) provides the DF level that reflects the Gibbs free energy of the [Y_Z^+ Q_a^- S_3^n] state (Fig. 5).

Fig. 4 shows that with increasing salt concentrations, first a decrease of τ_{O2} is observed which is followed by a relatively steep increase. The valence of the chloride cations appears to determine the onset concentration of increase and decrease in τ_{O2} with drastically lowered onset concentrations at increased cation valence. We conclude that the salt effect on τ_{O2} (Fig. 4) is qualitatively similar to the salt influence on the miss factor (Fig. 2). Increasing the salt concentration results first in enhanced functionality with increased transition efficiency and faster dioxygen formation and then, at high salt concentrations, in reduced functionality. The dependency on the cation valence suggests that in both cases electrostatic screening of negatively charged groups of the PSII proteins is involved.

3.4. Free-energy difference of proton-removal step

We noted above, in the qualitative discussion of the DF transient for the 3rd flash, that the salt concentration affects the energy level of the [Y_Z^+ Q_a^- S_3^n] state. Tri-exponential simulations with (Eq. (3)) facilitated a quantitative determination of the DF level (A_{ms}) that corresponds to the [Y_Z^+ Q_a^- S_3^n] state. The salt-concentration dependencies of the resulting values of A_{ms} are shown in Fig. 5. As the initial energy level of the [Y_Z^+ Q_a^- S_3^+] state was salt-independent (Fig. 3A), the decrease in A_{ms} corresponds to an increase in the free-energy difference associated with proton removal from the Mn-complex in the $S_3^+ \rightarrow S_3^n$ transition. Calculation of the corresponding Δ*G*-value is facilitated by Eq. (4). We note that also energetic relaxation at the donor side of PSII might contribute to the observable free-energy drop.

As opposed to the miss factor (Fig. 2) and the time constant of dioxygen formation (Fig. 4), a distinctively biphasic dependence of A_{ms} on the salt-concentration is not observed (Fig. 5). Nonetheless, it is conceivable that both, a specific low-concentration as well as a specific

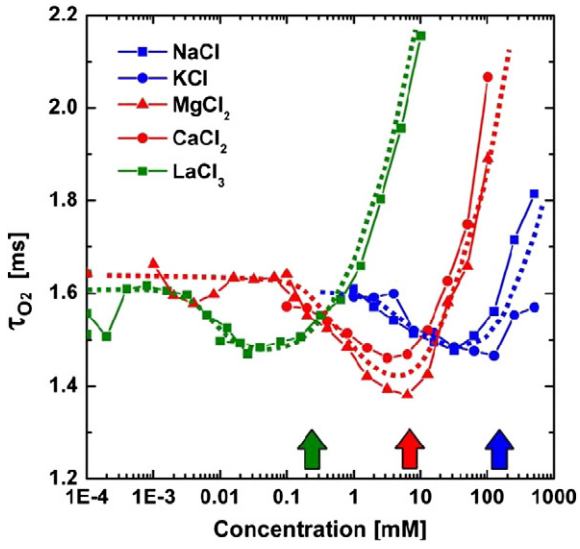

Fig. 4. Time constant of dioxygen formations step (τ_{O2}) at various salt concentrations. The value of τ_{O2} was obtained by a tri-exponential fit of the DF transients recorded after the 3rd-flash. The dotted lines do not represent any specific mathematical function, but were drawn to guide the eye. To facilitate comparison of the concentration dependencies, the positions of the colored marker arrows are identical to the respective positions in Fig. 2. Color coding: green: trivalent cation (La^{3+}), red: bivalent cations (Mg^{2+}, Ca^{2+}), blue: monovalent cations (Na^+, K^+).

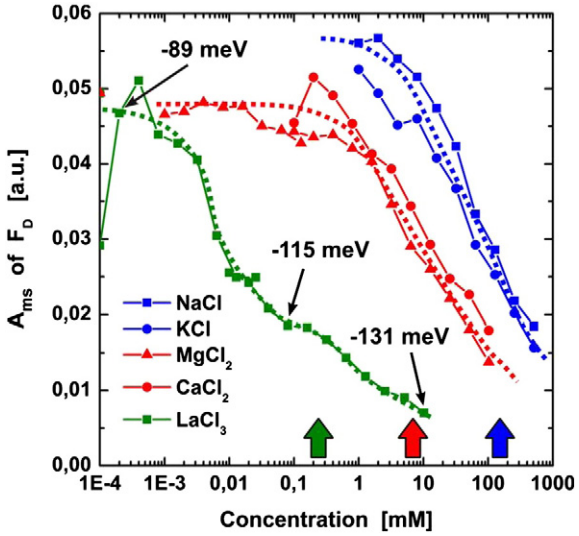

Fig. 5. Intensity of the delayed PSII fluorescence before onset of O_2-formation step. The amplitude (A_{ms}) of the millisecond component (τ_{O2}) of the tri-exponential simulation of the 3rd-flash DF transient is displayed. The value of A_{ms} relates closely to the Gibbs free-energy difference of the $S_3^+ \rightarrow S_3^n$ transition, which is indicated for minimal, intermediate, and maximal $LaCl_3$ concentration (calculated by Eq. (4)). We note that differences in the low-salt levels of A_{ms} likely result from minor variations in the properties of the used PSII preparations. To facilitate comparison of the concentration dependencies, the positions (on the concentration axis) of the colored marker arrows are identical to the respective positions in Fig. 2. Color coding: green: trivalent cation (La^{3+}), red: bivalent cations (Mg^{2+}, Ca^{2+}), blue: monovalent cations (Na^+, K^+).

high-concentration cation effect on A_{ms}, exist. A clear discrimination may be impossible because both effects result in decreasing A_{ms} for increasing salt concentration. In the case of the trivalent cation (La^{3+}), the plateau phase observed around 0.1 mM supports a biphasic concentration dependence.

A decrease in A_{ms} by 20% is reached at about 4 μM for the trivalent cation, 3 mM for the bivalent cations, and 20 mM for the monovalent cations. This cation-valence dependence suggests that electrostatic screening of negatively charged groups affects the change in Gibbs free energy associated with proton removal in the $S_3^+ \rightarrow S_3^n$ transition. The concentration dependence of the bivalent cations, however, appears to be special. In comparison to Fig. 2 and 4, a shift to clearly higher concentrations of the bivalent cation is observed. This may relate to interference of an electrostatic screening effect with binding of bivalent cations to specific protein sites. The presence of such binding sites is suggested by the identification of protein-internal calcium binding sites by means of protein crystallography [47,14].

3.5. Acceptor-side electron transfer

Within about 300 ps after chlorophyll excitation, the primary quinone acceptor, Q_a, is reduced and Q_a^- is formed. The yield of chlorophyll fluorescence is high in the presence of reduced Q_a and low in the presence of oxidized Q_a [38]. This variability of the fluorescence yield likely results from both, (i) a shift of the free energy level of the primary radical pair [Phe^-, $P680^+$] caused by an electrostatic interaction with the negatively charged Q_a^- and (ii) increased (ultra-fast) delayed fluorescence after formation of the primary radical pair resulting from blockade of the secondary electron transfer in the presence of reduced Q_a [48,38].

The fluorescence level is denoted as F_m, if reduced Q_a (Q_a^-) is present in all PSII complexes, whereas it is denoted as F_0 if Q_a is oxidized in all PSII. If Q_a^- is present in only a fraction of PSII, an intermediate fluorescence level (F_P) is detected which reflects the fraction of PSII with reduced Q_a. For a homogeneous PSII population and in the absence of excitation energy transfer between PSII units, the following relation holds [38]:

$$Q(t) = \frac{[Q_a^-](t)}{([Q_a^-] + [Q_a^{ox}])} = \left(\frac{F_P(t) - F_0}{F_M - F_0}\right) \quad (6)$$

Due to excitation energy transfer between neighboring PSII units, the relation between $[Q_a^-](t)$ and $F_P(t)$ may be more complex than indicated by Eq. (5) [38,49], but this can be neglected for the semi-quantitative analysis of the fluorescence-detected Q_a^- time course as applied herein.

After excitation with a saturating laser flash, a maximal fluorescence level is reached ($Q(t) = 1$) followed by subsequent decay of $F_P(t)$ resulting from Q_a^- re-oxidation. In Fig. 6A, $Q(t)$ is shown for various salt concentrations. Simulations with a sum of exponential functions have revealed that the Q_a^- re-oxidation is at least tri-phasic [50]. The rapid phase ($t < 10$ ms) has been assigned to electron transfer from Q_a^- to firmly bound Q_b. However, Q_b may not be appropriately bound to all PSII so that the intermediate phase (10 ms–100 ms) has been assigned to binding of Q_b followed by rapid $Q_a^- \rightarrow Q_b$ electron transfer. The slowest phase ($t > 100$ ms) likely is dominated by charge recombination between reduced quinones and oxidized redox factors at the PSII donor side. Because simulations do not necessarily facilitate a clear-cut separation of these decay phases, we restrict our analysis to the halftime of the $Q(t)$ decay (Fig. 6B). (We note that in comparison to preparations of thylakoid membranes (broken chloroplasts) [51], the reactions at the PSII acceptor side are reproducibly slowed down in preparations of PSII membrane particles. This likely is explainable by a detergent influence on the quinone binding sites [52], in line with crystallographic data (i) showing the presence of detergent molecules in the PSII core complex and (ii) suggesting that specifically the quinone binding sites are well accessible to detergent molecules [53,54].)

Visual inspection of the time courses shown in Fig. 6A immediately reveals a strong salt-influence on the Q_a^- reoxidation. At longer times (>100 ms), little difference is observable suggesting that the recombination reaction is not affected, but the electron transfer from Q_a^- to the secondary quinone acceptor, Q_b. (Employing time-resolved infrared spectroscopy, we found that the electron is transferred first to Q_b and only later to the artificial electron acceptor; unpublished results.) Most likely both, the electron transfer to quinone molecules properly bound at the Q_b site is affected as well as the binding of Q_b. However, also by multi-exponential simulations a clear-cut separation of these two phenomena cannot be achieved. Therefore, we revert to a simplified analysis, that is, evaluation of the decay-halftime of the prompt fluorescence yield. The halftimes for five salts are shown in Fig. 6B. Similar to the data shown in Fig. 2 and 4, biphasic concentration dependence is observed. Only in the case of $LaCl_3$, the rise in the halftime observed at high concentrations is not detectable. The half-effect concentration of the stimulating salt effect is around 10 μM for the trivalent cation (La^{3+}), 200 μM for the bivalent cations (Mg^{2+}, Ca^{2+}), and 10 mM for the monovalent cations (Na^+, K^+). Again, the half-effect concentration depends strongly on the cation valence suggesting that also this salt-effect on the acceptor-side electron transfer originates from electrostatic screening of negatively charged surface groups.

4. Discussion

4.1. Cationic screening of surface carboxylates

In the time-resolved experiments described above, we detected a clear influence of salts on specific reactions at the donor and at the acceptor side of PSII. Chloride salts with monovalent, bivalent and trivalent cations were used and the cation concentrations required to observe the effect on the PSII reactions depended strongly on the cation valence with $C^{3+} \gg C^{2+} \gg C^{1+}$, and was independent of the ion size. This behavior indicates electrostatic screening of negative charges at the solvent-exposed protein surface, as described in the Section 1

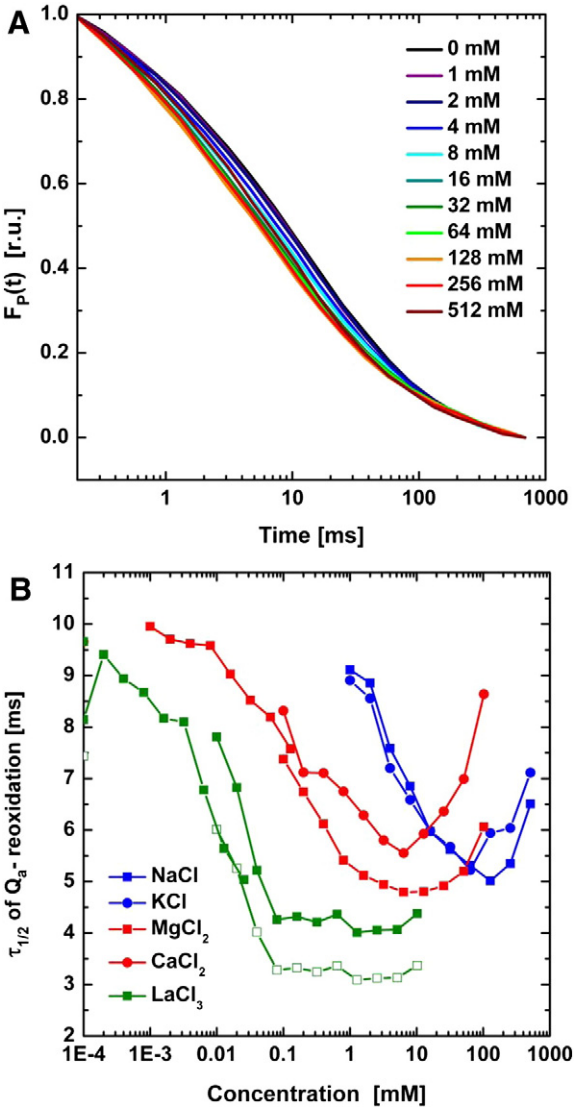

Fig. 6. Salt influence on the Q_a^- reoxidation after application of a saturating laser flash to dark-adapted PSII membrane particles (1.5 mJ/cm^2, 532 nm, 5 ns FWHM). The kinetics of Q_a^- reoxidation are tracked via detection of the variable yield of prompt chlorophyll fluorescence. In A, normalized time courses for eleven NaCl concentrations are shown; each curves represents the average of five measurements. In B, concentrations dependencies of the halftimes of the decay curves (of the normalized $F_P(t)$) for five salts. For $LaCl_3$, one low-concentration series ([$LaCl_3$] < 40 μM) and one high-concentration series ([$LaCl_3$] > 10 μM) were acquired. Obviously their halftimes do not match well in the overlapping concentration regime, likely explainable by the variability of the used plant material. After normalization to equal zero-salt levels (open green squares), the high-concentration series and of low-concentration series match up well. To facilitate comparison of the concentration dependencies, the selected positions (on the concentration axis) of the colored marker arrows are identical to the respective positions in Fig. 2. Color coding: green, trivalent cation (La^{3+}); red, bivalent cations (Mg^{2+}, Ca^{2+}); blue, monovalent cations (Na^+, K^+).

Introduction. Such a dependence on the cation valence and the absence of ion size effects are incompatible with binding of cations to specific sites inside the protein.

Are there other explanations? The chloride concentrations we used for investigating the influence of trivalent, bivalent and monovalent cations differed by orders of magnitude; this excludes any major chloride-specific effect. Nonetheless, modification of the cation concentration dependency by an overlapping chloride effects cannot be excluded definitively, especially at high concentrations of the monovalent anion.

The ion-exposure periods had been relatively short in our experiments. Nonetheless, the exposure to aqueous buffers of high ionic strength might affect the integrity of the PSII donor side by depletion of extrinsic polypeptides coupled to release of calcium and or manganese [55–65]. In past work, we have investigated the depletion of extrinsic polypeptides using activity assays, gel electrophoresis and delayed fluorescence experiments [63–65]. In these investigations, we found that the delayed fluorescence reacts extremely sensitive to any depletion of extrinsic PSII polypeptides, calcium or manganese—far more sensitive than, e.g., integrity assessment by gel electrophoresis. For example, the data shown in Fig. 1 would look clearly modified even for a minor fraction of detrimentally affected PSII (see [63–66,34,67]). Thus we can essentially exclude the above secondary ion effects.

The dependence of specific reactions on the cation valence can be discussed in terms of the Gouy–Chapman theory for a homogeneous negative charge density at a planar solvent-exposed surface (see Section 1 Introduction). In contrast to the simple, homogeneous distribution of ions considered in the Gouy–Chapman theory, the solvent-exposed surfaces of PSII exhibit a complex distribution of negatively charged carboxylate groups (Fig. 7). There are numerous carboxylates at both the stroma and lumen surfaces; some of these carboxylates are located within close distances, that is, they form clusters, whereas other carboxylates are scattered across regions of the protein surface rich in both carboxylate- and positively-charged groups (Fig. 7). The charged groups at the stroma and lumen sides of PSII can participate in complex networks of hydrogen bonds (see examples in Fig. 8, S1, S2, and ref. [25,26]) that likely have a significant effect on the dynamics of water and ions close to the protein surface.

The remarkable number of surface-exposed Asp and Glu sidechains of PSII suggests that the cation dependence we observe here is related to the electrostatic screening of such carboxylates. The complex

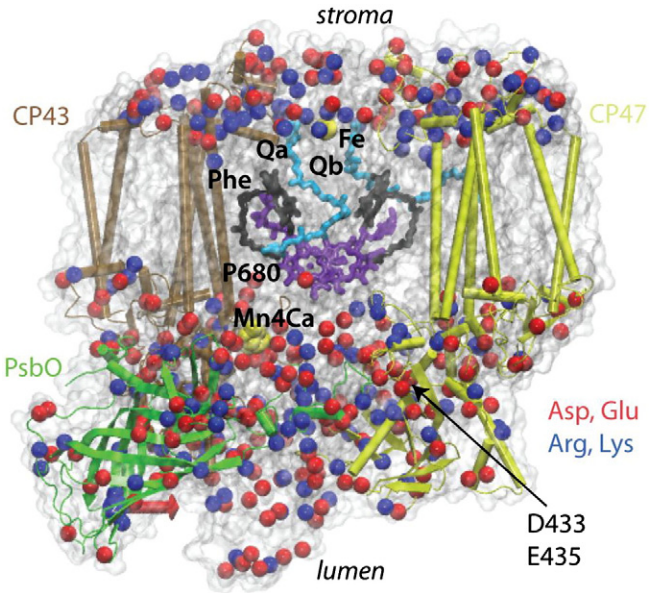

Fig. 7. Distribution of charged groups in *T. vulcanus* PSII. The image is based on the crystallographic model of Umena et al. [14] (PDB ID:3ARC, molecule A). Cα atoms of negatively-charged groups (Asp/Glu) are depicted as red spheres, and Cα atoms of positively-charged groups (Arg/Lys) as blue spheres. The oxygen-evolving complex (Mn_4Ca) is shown as yellow surface; other redox factors are depicted as bonds (P680, purple; Phe, brown; Q_a and Q_b, cyan), and the iron on the stroma side is shown as a yellow sphere. The redox-active tyrosine Y_Z located close to oxygen-evolving complex is not shown. The CP43 and CP47 subunits are shown as brown and yellow cartoons, respectively, and the extrinsic PsbO subunit is in green. The arrow indicates the location of an inter-subunit carboxylate cluster that involves D433 and E435 of CP47 [25,26]. We used VMD (Humphrey et al. 1996) for the molecular graphics images in Fig. 7 and 8.

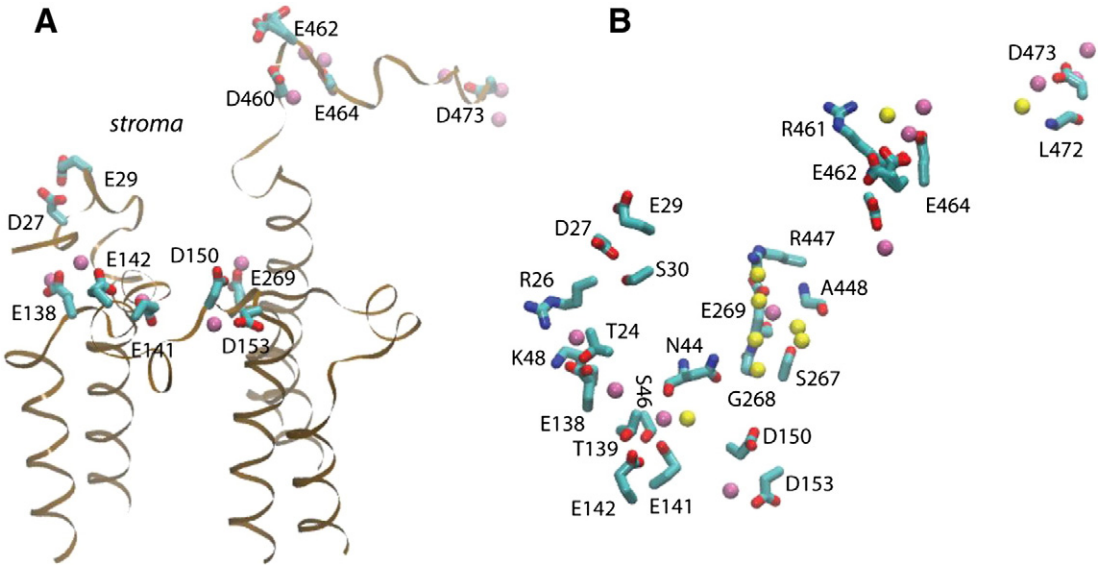

Fig. 8. Carboxylate groups at the stroma side of the CP43 subunit. (A) Aspartate and glutamate amino acid residues on the stroma side of CP43. Oxygen atoms of water molecules within 3.5 Å of the carboxylate oxygen atoms are shown as purple spheres. (B) Close view of the stroma side of CP43. Yellow spheres indicate oxygen atoms of other hydrogen-bonded water molecules that are not within 3.5 Å of the carboxylate groups, some of which being within 3.5 Å of waters hydrogen bonded to the carboxylates. Fig. 7 and 8 were prepared based on the *T. vulcanus* crystal structure by Umena et al. [14]. A brief analysis of the similarity between the sequences of CP43, CP47, and PsbO from *T. vulcanus* and spinach PSII is provided in the Supporting information.

distribution of the surface carboxylate and positively charged groups (Fig. 7) hinders the straightforward application of the Gouy–Chapman theory to quantify the effect of the surface charges on the cations tested herein. Nevertheless, the Gouy–Chapman theory does allow for a qualitative understanding of how the cation valence affects the strength of cation screening and the magnitude of the surface potential.

4.2. Interaction between surface charges and protein interior

How could the cation screening of negative surface charges affect processes in the protein interior? In vicinity of charged surface groups, a negative electric surface potential is expected. For a solvent phase with high cationic strength, this electric potential will decrease rapidly for increasing distances from the membrane (e.g., half-decay length of 5 Å); but the potential will decrease clearly more slowly if screening by dissolved cations is absent (e.g., half-decay length of 30 Å). Moreover, cationic screening will decrease the effective surface-charge density at the protein surface. The influence of cations on strength and decay length of the negative surface potential is a crucial determinant of thylakoid stacking, but is not predicted to affect inner-protein processes directly. Regarding reactions in the protein interior, the extent of diminishment of surface potentials by cationic screening could be the decisive factor. Especially for clusters of negatively charged surface groups, the resulting negative surface potentials could affect processes in the protein interior that are tens of Angstroms away. The electrostatic potential resulting from negative surface charges will render redox potentials more negative and decrease p*K* values of protonatable groups in the protein interior (by about one p*K* unit per 60 mV of electrostatic potential at the protonation site).

The cation screening of charged carboxylates could affect the surface charge also via a second route. The p*K* for protonation of asparte and glutamate side chains in aqueous solution is predicted to be around 4 so that in our experiments at pH 6.2, all surface-exposed carboxylates might be predicted to be unprotonated. Yet within a cluster of negatively charged carboxylates, mutual electrostatic interactions may favor partial protonation of the carboxylate cluster, even at pH 6.2. Now electrostatic cation screening could promote deprotonation, thereby increasing the negative charge of the carboxylate cluster. This means that at high cation concentrations, there are two opposing influences on the effective negative surface charge: cation screening tends to reduce the surface charge, whereas cation-induced deprotonation could increase it. The interrelation between electrostatic screening and protonation of surface groups has been discussed also for the thylakoid stacking [29].

4.3. Possible regulatory role

Cationic screening of surface charges affects the transition efficiency (miss factor), which is determined by the competition between forward reactions (at donor and acceptor side of PSII) and losses due to recombination processes [68–71,37,72]. Several recombination routes are involved [71,72] and their relative importance is regulated at the transcriptional level via control of the relative proportions of variants of the PsbA gene product (D1 protein) [73–79]. On a first glance, the functional difference between the various PsbA gene products appears to be relatively minor. Nonetheless, this genetic regulation most likely supports adaptation to various environmental conditions significantly. We consider it possible that also the herein reported functional changes that result from variation in the cationic screening of surface groups are involved in adaptation of PSII to excessive light-intensities (photoprotection) or other variations of environmental conditions. In higher plants, a close and potentially synergistic relation to light adaptation by control of thylakoid stacking [30] could be envisioned.

It represents a central (and surprising) results of our study that electrostatic screening of negatively charged surface groups, most likely carboxylate side chains, affects relatively distant electron transfer reactions in the interior of the protein complex significantly. In PSII, the presence of significant long-distance interaction between protein-internal redox factors (Y_Z and the Mn_4Ca complex) and the protonation state of peripheral groups has been postulated before in order to explain the pH-dependent, non-integer proton release associated with the individual S-state transitions [80–82,4]. Especially Junge and coworkers have provided evidence that upon oxidation of the redox-active tyrosine (Y_Z), long-range electrostatic interactions cause deprotonation of groups at the periphery (or surface) of PSII [83,84,4]. We consider our investigation to be a starting point for further investigations on the control (or coordination) of PSII function by long-range interactions. The functional or regulatory role of interactions between protein surface and protein interior represents an aspect of protein function that, in our opinion, requires clearly more in-depth investigation.

Acknowledgements

We thank Dr. Ivelina Zaharieva who promoted the prompt and delayed fluorescence experiments significantly, inter alia by development of data evaluation software. We thank Dr. Michael Haumann for the insightful discussion. The collaborative research center on 'Protonation dynamics in protein function' (SFB 1078) funded by the Deutsche Forschungsgemeinschaft (DFG) supported this research via projects A4 (to H.D.) and C4 (to A.-N.B.). A.-N.B. is supported in part by the Marie Curie International Reintegration Award IRG-276920. Initial work in the lab of H.D. was supported within the framework of the 'H2-design cell' consortium by the Bundesministerium für Bildung und Forschung (BMBF, #03SF0355D).

Appendix A. Supplementary data

Supplementary data to this article can be found online at http://dx.doi.org/10.1016/j.bbabio.2014.07.012.

References

[1] D. Ort, C.F. Yocum, Oxygenic Photosynthesis: The Light Reactions, Kluwer Academic Publ, Dordrecht, 1996.
[2] R.E. Blankenship, Molecular Mechanisms of Photosynthesis, Blackwell Science, Oxford, England, 2002.
[3] B. Ke, Photosynthesis — Photobiochemistry and Photobiophysics, Kluwer Academic Publishers, Dordrecht, 2001.
[4] W. Junge, M. Haumann, R. Ahlbrink, A. Mulkidjanian, J. Clausen, Electrostatics and proton transfer in photosynthetic water oxidation, Phil. Trans. R. Soc. B 357 (2002) 1407–1418.
[5] J.P. McEvoy, G.W. Brudvig, Water-splitting chemistry of photosystem II, Chem. Rev. 106 (2006) 4455–4483.
[6] G. Renger, T. Renger, Photosystem II: the machinery of photosynthetic water splitting, Photosynth. Res. 98 (2008) 53–80.
[7] J. Barber, Photosynthetic energy conversion: natural and artificial, Chem. Soc. Rev. 38 (2009) 185–196.
[8] H. Dau, I. Zaharieva, Principles, efficiency, and blueprint character of solar-energy conversion in photosynthetic water oxidation, Acc. Chem. Res. 42 (2009) 1861–1870.
[9] H. Dau, I. Zaharieva, M. Haumann, Recent developments in research on water oxidation by photosystem II, Curr. Opin. Chem. Biol. 16 (2012) 3–10.
[10] S. Styring, J. Sjöholm, F. Mamedov, Two tyrosines that changed the world: Interfacing the oxidizing power of photochemistry to water splitting in photosystem II, Biochim. Biophys. Acta 1817 (2012) 76–87.
[11] A. Zouni, H.T. Witt, J. Kern, P. Fromme, N. Krauss, W. Saenger, P. Orth, Crystal structure of photosystem II from *Synechococcus elongatus* at 3.8 Å resolution, Nature 409 (2001) 739–743.
[12] K.N. Ferreira, T.M. Iverson, K. Maghlaoui, J. Barber, S. Iwata, Architecture of the photosynthetic oxygen-evolving center, Science 303 (2004) 1831–1838.
[13] B. Loll, J. Kern, W. Saenger, A. Zouni, J. Biesiadka, Towards complete cofactor arrangement in the 3.0 Å resolution structure of photosystem II, Nature 438 (2005) 1040–1044.
[14] Y. Umena, K. Kawakami, J.-R. Shen, N. Kamiya, Crystal structure of oxygen-evolving photosystem II at a resolution of 1.9 Å, Nature 473 (2011) 55–60.
[15] H. Dau, M. Haumann, Reaction cycle of photosynthetic water oxidation in plants and cyanobacteria (response letter), Science 312 (2006) 1471–1472.
[16] H. Dau, M. Haumann, Eight steps preceding O – O bond formation in oxygenic photosynthesis—a basic reaction cycle of the photosystem II manganese complex, Biochim. Biophys. Acta 1767 (2007) 472–483.
[17] A. Klauss, M. Haumann, H. Dau, Alternating electron and proton transfer steps in photosynthetic water oxidation, Proc. Natl. Acad. Sci. U. S. A. 109 (2012) 16035–16040.
[18] W. Arnold, The ration between delayed light and fluorescence emitted by chloroplasts, Biophys. J. 12 (1972) 793–796.
[19] A.A. Bulychev, V.K. Andrianov, G.A. Kurella, F.F. Litvin, Photoinduction kinetics of electrical potential in a single chloroplast as studied with micro-electrode technique, Biochim. Biophys. Acta 430 (1976) 336–351.
[20] J.L. Ellenson, K. Sauer, The electrophotoluminescence of chloroplasts, Photochem. Photobiol. 23 (1976) 113–123.
[21] P.S. Venediktov, V.N. Goltsev, V.P. Shinkarev, The influence of the electric diffusion potential on delayed fluorescence light curves of chloroplasts treated with 3-(3,4-dichlorophenyl)-1,1-dimethylurea, Biochim. Biophys. Acta 593 (1980) 125–132.
[22] R.F. Meiburg, H.J. van Gorkom, R.J. van Dorssen, Excitation trapping and charge separation in photosystem II in the presence of an electrical field, Biochim. Biophys. Acta 724 (1983) 352–358.
[23] H. Dau, R. Windecker, U.P. Hansen, Effect of light-induced changes in thylakoid voltage on chlorophyll fluorescence of *Aegopodium podagraria* leaves, Biochim. Biophys. Acta 1057 (1991) 337–345.
[24] H. Dau, K. Sauer, Electric field effect on the picosecond fluorescence of photosystem II and its relation to the energetics and kinetics of primary charge separation, Biochim. Biophys. Acta 1102 (1992) 91–106.
[25] T. Shutova, V.V. Klimov, B. Andersson, G. Samuelsson, A cluster of carboxylic groups in PsbO protein is involved in proton transfer from the water oxidizing complex of photosystem II, Biochim. Biophys. Acta 1767 (2007) 434–440.
[26] A.N. Bondar, H. Dau, Extended protein/water H-bond networks in photosynthetic water oxidation, Biochim. Biophys. Acta 1817 (2012) 1177–1190.
[27] S. Murakami, L. Packer, The role of cations in the organization of chloroplast membranes, Arch. Biochem. Biophys. 146 (1971) 337–347.
[28] J. Barber, G.F.W. Searle, Cation induced increase in chlorophyll fluorescence yield and effect of electrical charge, FEBS Lett. 92 (1978) 5–8.
[29] J. Barber, Membrane surface charges and potentials in relation to photosynthesis, Biochim. Biophys. Acta 594 (1980) 253–308.
[30] J.M. Anderson, W.S. Chow, J. De Las Rivas, Dynamic flexibility in the structure and function of photosystem II in higher plant thylakoid membranes: the grana enigma, Photosynth. Res. 98 (2008) 575–587.
[31] G. Cevc, Membrane electrostatics, Biochim. Biophys. Acta 1031 (1990) 311–382.
[32] M. Grabolle, H. Dau, Energetics of primary and secondary electron transfer in photosystem II membrane particles of spinach revisited on basis of recombination-fluorescence measurements, Biochim. Biophys. Acta 1708 (2005) 209–218.
[33] J. Buchta, M. Grabolle, H. Dau, Photosynthetic dioxygen formation studied by time-resolved delayed fluorescence measurements—method, rationale, and results on the activation energy of dioxygen formation, Biochim. Biophys. Acta 1767 (2007) 565–574.
[34] R. Krivanek, J. Kern, A. Zouni, H. Dau, M. Haumann, Spare quinones in the Q_B cavity of crystallized photosystem II from *Thermosynechococcus elongatus*, Biochim. Biophys. Acta 1767 (2007) 520–527.
[35] L. Iuzzolino, J. Dittmer, W. Dörner, W. Meyer-Klaucke, H. Dau, X-ray absorption spectroscopy on layered photosystem II membrane particles suggests manganese-centered oxidation of the oxygen-evolving complex for the S_0–S_1, S_1–S_2, and S_2–S_3 transitions of the water oxidation cycle, Biochemistry 37 (1998) 17112–17119.
[36] H. Schiller, H. Dau, Preparation protocols for high-activity photosystem II membrane particles of green algae and higher plants, pH dependence of oxygen evolution and comparison of the S_2-state multiline signal by X-band EPR spectroscopy, J. Photochem. Photobiol. B 55 (2000) 138–144.
[37] M. Grabolle, H. Dau, Efficiency and role of loss processes in light-driven water oxidation by PSII, Physiol. Plant. 131 (2007) 50–63.
[38] H. Dau, Molecular mechanisms and quantitative models of variable photosystem II fluorescence, Photochem. Photobiol. 60 (1994) 1–23.
[39] P. Joliot, A. Joliot, Analysis of the interactions between the two photosystems in isolated chloroplasts, Biochim. Biophys. Acta 153 (1968) 635–652.
[40] B. Kok, B. Forbush, M. McGloin, Cooperation of charges in photosynthetic O_2 evolution — I. A linear four-step mechanism, Photochem. Photobiol. 11 (1970) 457–475.
[41] H. Dau, M. Haumann, Time-resolved X-ray spectroscopy leads to an extension of the classical S-state cycle model of photosynthetic oxygen evolution, Photosynth. Res. 92 (2007) 327–343.
[42] M. Haumann, P. Liebisch, C. Muller, M. Barra, M. Grabolle, H. Dau, Photosynthetic O_2 formation tracked by time-resolved X-ray experiments, Science 310 (2005) 1019–1021.
[43] L. Gerencser, H. Dau, Water oxidation by photosystem II: H_2O–D_2O exchange and the influence of ph support formation of an intermediate by removal of a proton before dioxygen creation, Biochemistry 49 (2010) 10098–10106.
[44] I. Zaharieva, M. Grabolle, P. Chernev, H. Dau, Water oxidation in photosystem II: Energetics and kinetics of intermediates formation in $S_{2-} > S_3$ and $S_{3-} > S_0$ transitions monitored by delayed chlorophyll fluorescence, in: T. Kuang, C. Lu, L. Zhang (Eds.), Photosynthesis Research for Food, Fuel and Future, Springer, Heidelberg, 2013, pp. 234–238.
[45] H. Dau, M. Haumann, The manganese complex of photosystem II in its reaction cycle—basic framework and possible realization at the atomic level, Coord. Chem. Rev. 252 (2008) 273–295.
[46] F. Rappaport, M. Blanchard-Desce, J. Lavergne, Kinetics of electron transfer and electrochromic change during the redox transition of the photosynthetic oxygen-evolving complex, Biochim. Biophys. Acta 1184 (1994) 178–192.
[47] J.W. Murray, J. Barber, Identification of a calcium-binding site in the PsbO protein of photosystem II, Biochemistry 45 (2006) 4128–4130.
[48] G.H. Schatz, H. Brock, A.R. Holzwarth, Kinetic and energetic model for the primary processes in photosystem II, Biophys. J. 54 (1988) 397–405.
[49] J. Lavergne, H.W. Trissl, Theory of fluorescence induction in photosystem II: derivation of analytical expressions in a model including exciton-radical-pair equilibrium and restricted energy transfer between photosynthetic units, Biophys. J. 68 (1995) 2474–2492.
[50] R. de Wijn, H.J. van Gorkom, Kinetics of electron transfer from Q_a to Q_b in photosystem II, Biochemistry 40 (2001) 11912–11922.
[51] J.M. Bowes, A.R. Crofts, Binary oscillations in the rate of reoxidation of the primary acceptor of photosystem II, Biochim. Biophys. Acta 590 (1980) 373–384.
[52] J. Kurreck, R. Schodel, G. Renger, Investigation of the plastoquinone pool size and fluorescence quenching in thylakoid membranes and photosystem II (PS II) membrane fragments, Photosynth. Res. 63 (2000) 171–182.
[53] A. Guskov, J. Kern, A. Gabdulkhakov, M. Broser, A. Zouni, W. Saenger, Cyanobacterial photosystem II at 2.9-Å resolution and the role of quinones, lipids, channels and chloride, Nat. Struct. Mol. Biol. 16 (2009) 334–342.
[54] F. Muh, C. Glockner, J. Hellmich, A. Zouni, Light-induced quinone reduction in photosystem II, Biochim. Biophys. Acta 1817 (2012) 44–65.
[55] D.F. Ghanotakis, G.T. Babcock, C.F. Yocum, Calcium reconstitutes high-rates of oxygen evolution in polypeptide depleted photosystem-ii preparations, FEBS Lett. 167 (1984) 127–130.
[56] D.F. Ghanotakis, G.T. Babcock, C.F. Yocum, Structural and catalytic properties of the oxygen-evolving complex — correlation of polypeptide and manganese release

with the behavior of Z + In chloroplasts and a highly resolved preparation of the ps-ii complex, Biochim. Biophys. Acta 765 (1984) 388–398.
[57] R.J. Debus, The manganese and calcium ions of photosynthetic oxygen evolution, Biochim. Biophys. Acta 1102 (1992) 269–352.
[58] T.A. Ono, S. Izawa, Y. Inoue, Structural and functional modulation of the manganese cluster in Ca^{2+}-depleted photosystem II induced by binding of the 24-kilodalton extrinsic protein, Biochemistry 31 (1992) 7648–7655.
[59] W. Hillier, T. Wydrzynski, Increases in peroxide formation by the photosystem II oxygen evolving reactions upon removal of the extrinsic 16, 22 and 22 kDa proteins are reversed by $CaCl_2$ addition, Photosynth. Res. 38 (1993) 417–423.
[60] L.E. Andreasson, I. Vass, S. Styring, Ca^{2+} depletion modifies the electron-transfer on both donor and acceptor sides in photosystem II from spinach, Biochim. Biophys. Acta 1230 (1995) 155–164.
[61] C. Tommos, J. McCracken, S. Styring, G.T. Babcock, Stepwise disintegration of the photosynthetic oxygen-evolving complex, J. Am. Chem. Soc. 120 (1998) 10441–10452.
[62] W. Hillier, G. Hendry, R.L. Burnap, T. Wydrzynski, Substrate water exchange in photosystem II depends on the peripheral proteins, J. Biol. Chem. 276 (2001) 46917–46924.
[63] P. Pospíšil, M. Haumann, J. Dittmer, V.A. Solé, H. Dau, Stepwise transition of the tetra-manganese complex of photosystem II to a binuclear $Mn_2(\mu\text{-}O)_2$ complex in response to a temperature jump: a time resolved structural investigation employing X-ray absorption spectroscopy, Biophys. J. 84 (2003) 1370–1386.
[64] M. Barra, M. Haumann, H. Dau, Specific loss of the extrinsic 18 kDa protein from photosystem II upon heating to 47 °C causes inactivation of oxygen evolution likely due to Ca release from the Mn-complex, Photosynth. Res. 84 (2005) 231–237.
[65] M. Barra, M. Haumann, P. Loja, R. Krivanek, A. Grundmeier, H. Dau, Intermediates in assembly by photoactivation after thermally accelerated disassembly of the manganese complex of photosynthetic water oxidation, Biochemistry 45 (2006) 14523–14532.
[66] M. Haumann, M. Barra, P. Loja, S. Loscher, R. Krivanek, A. Grundmeier, L.E. Andreasson, H. Dau, Bromide does not bind to the Mn_4Ca complex in its S_1 state in Cl^--depleted and Br^--reconstituted oxygen-evolving photosystem II: evidence from X-ray absorption spectroscopy at the Br K-edge, Biochemistry 45 (2006) 13101–13107.
[67] M. Haumann, A. Grundmeier, I. Zaharieva, H. Dau, Photosynthetic water oxidation at elevated dioxygen partial pressure monitored by time-resolved X-ray absorption measurements, Proc. Natl. Acad. Sci. U. S. A. 105 (2008) 17384–17389.
[68] V.P. Shinkarev, C.A. Wraight, Oxygen evolution in photosynthesis: from unicycle to bicycle, Proc. Natl. Acad. Sci. U. S. A. 90 (1993) 1834–1838.
[69] R. de Wijn, H.J. van Gorkom, The rate of charge recombination in photosystem II, Biochim. Biophys. Acta 1553 (2002) 302–308.
[70] F. Rappaport, M. Guergova-Kuras, P.J. Nixon, B.A. Diner, J. Lavergne, Kinetics and pathways of charge recombination in photosystem II, Biochemistry 41 (2002) 8518–8527.
[71] K. Cser, I. Vass, Radiative and non-radiative charge recombination pathways in photosystem II studied by thermoluminescence and chlorophyll fluorescence in the cyanobacterium *Synechocystis* 6803, Biochim. Biophys. Acta 1767 (2007) 233–243.
[72] I. Vass, K. Cser, Janus-faced charge recombinations in photosystem II photoinhibition, Trends Plant Sci. 14 (2009) 200–205.
[73] P.B. Kos, Z. Deak, O. Cheregi, I. Vass, Differential regulation of psbA and psbD gene expression, and the role of the different D1 protein copies in the cyanobacterium *Thermosynechococcus elongatus* BP-1, Biochim. Biophys. Acta 1777 (2008) 74–83.
[74] C.I. Sicora, C.M. Brown, O. Cheregi, I. Vass, D.A. Campbell, The psbA gene family responds differentially to light and UVB stress in *Gloeobacter violaceus* PCC 7421, a deeply divergent cyanobacterium, Biochim. Biophys. Acta 1777 (2008) 130–139.
[75] T.C. Summerfield, J. Toepel, L.A. Sherman, Low-oxygen induction of normally cryptic psbA genes in cyanobacteria, Biochemistry 47 (2008) 12939–12941.
[76] P. Mulo, C. Sicora, E.M. Aro, Cyanobacterial psbA gene family: optimization of oxygenic photosynthesis, Cell. Mol. Life Sci. 66 (2009) 3697–3710.
[77] J. Sander, M. Nowaczyk, J. Buchta, H. Dau, I. Vass, Z. Deák, M. Dorogi, M. Iwai, M. Rögner, Functional characterization and quantification of the alternative PsbA copies in *Thermosynechococcus elongatus* and their role in photoprotection, J. Biol. Chem. 285 (2010) 29851–29856.
[78] M. Sugiura, E. Iwai, H. Hayashi, A. Boussac, Differences in the interactions between the subunits of photosystem II dependent on D1 protein variants in the thermophilic cyanobacterium *Thermosynechococcus elongatus*, J. Biol. Chem. 285 (2010) 30008–30018.
[79] I. Sakurai, D. Stazic, M. Eisenhut, E. Vuorio, C. Steglich, W.R. Hess, E.M. Aro, Positive regulation of psbA gene expression by cis-encoded antisense RNAs in *Synechocystis* sp. PCC 6803, Plant Physiol. 160 (2012) 1000–1010.
[80] F. Rappaport, J. Lavergne, Proton release during successive oxidation steps of the photosynthetic water oxidation process: stoichiometries and pH dependence, Biochemistry 30 (1991) 10004–10012.
[81] J. Lavergne, W. Junge, Proton release during the redox cycle of the water oxidase, Photosynth. Res. 38 (1993) 279–296.
[82] E. Schlodder, H.T. Witt, Stoichiometry of proton release from the catalytic center in photosynthetic water oxidation. Reexamination by a glass electrode study at ph 5.5–7.2, J. Biol. Chem. 274 (1999) 30387–30392.
[83] M. Haumann, W. Junge, Extent and rate of proton release by photosynthetic water oxidation in thylakoids: electrostatic relaxation versus chemical production, Biochemistry 33 (1994) 864–872.
[84] R. Ahlbrink, M. Haumann, D. Cherepanov, O. Boegershausen, A. Mulkidjanian, W. Junge, Function of tyrosine-Z in water oxidation by photosystem II: electrostatical promotor instead of hydrogen abstractor, Biochemistry 37 (1998) 1131–1142.